

Coarsening dynamics of aster defects in a model polar active matter

Soumyadeep Mondal,^{1,*} Pankaj Popli,^{1,†} and Sumantra Sarkar^{1,‡}

¹*Center for Condensed Matter Theory, Department of Physics,
Indian Institute of Science, Bengaluru, Karnataka, India, 560012*

(Dated: November 11, 2024)

We numerically study the coarsening behavior of topological defects in 2D polar active matter. Our model captures the dynamics of actin aster organization in cell membranes. We also compare our results with experimental data. The model is given by,

$$\partial_t \mathbf{p} + \lambda(\mathbf{p} \cdot \nabla) \mathbf{p} = k_1 \nabla^2 \mathbf{p} + k_2 \nabla(\nabla \cdot \mathbf{p}) + (\alpha - \beta|\mathbf{p}|^2) \mathbf{p} + \zeta \nabla c + \mathbf{f}_p \quad (1)$$

$$\partial_t c = -\nabla \cdot (\mathbf{j}_a + \mathbf{j}_d) = -\nabla \cdot (v_0 c \mathbf{p} - D \nabla c) \quad (2)$$

Eq.1 describes the time evolution of the \mathbf{p} -field. Eq.2 is a continuity equation ensuring the conservation of the total number of particles in the system. The particles are transported through the active advective current (\mathbf{j}_a) and the passive diffusive current (\mathbf{j}_d). In Eq.1, the term with coefficient λ is a non-linear self-advection term that resembles the advection term in the Navier-Stokes equation. The first two terms on the right side of Eq.1 arise due to the elastic deformation (bending and splay terms) of the \mathbf{p} field, the third term ensures the stability of the \mathbf{p} -field through the parameter α and β and arises from the functional derivative of the Landau-Ginzburg free energy functional, the fourth term is an active term which couples the p -field with the c -filed via an active parameter called contractility ζ , The stochasticity in the system appears in the last term where \mathbf{f}_p is conservative noise in the system with noise strength T_a , called active temperature. Hence, it is delta correlated both in space and time $\langle \mathbf{f}_p(\mathbf{r}, t) \mathbf{f}_p'(\mathbf{r}', t') \rangle = T_a \delta(\mathbf{r} - \mathbf{r}') \delta(t - t')$. In Eq.2, the active term couples the two fields through the self-propulsion speed v_0 , which we take to be 1. Consequently, the system becomes active, with the concentration field coupled with the orientational field.

In the main text, we use a simplified model by setting $\lambda = k_2 = 0$ and relabeling k_1 as K .

$$\partial_t \mathbf{p} = K \nabla^2 \mathbf{p} + (\alpha - \beta|\mathbf{p}|^2) \mathbf{p} + \zeta \nabla c + \mathbf{f}_p \quad (3)$$

$$\partial_t c = -\nabla \cdot (v_0 c \mathbf{p} - D \nabla c) \quad (4)$$

In the SI, we explore the effect of these terms and show that they do not change the qualitative results. Also, we provide detailed analysis of some other aspects of the model.

THE EFFECT OF THE ACTIVE TEMPERATURE (T_a)

To investigate the effect of active temperature, we slowly vary the temperature from strength 1 to 10. We observe the same kind of coarsening dynamics of the defects by switching on these terms. However, increasing T_a leads to fragmentation of the asters, and the number of defects is higher as we increase the temperature T_a , similar to the unbinding of defects at higher temperatures in Kosterlitz-Thouless transition. Fig. 1. A trade-off exists between the contractility (ζ) and T_a . Increasing T_a leads to the fragmentation of the asters, and contractility encourages the formation of the asters.

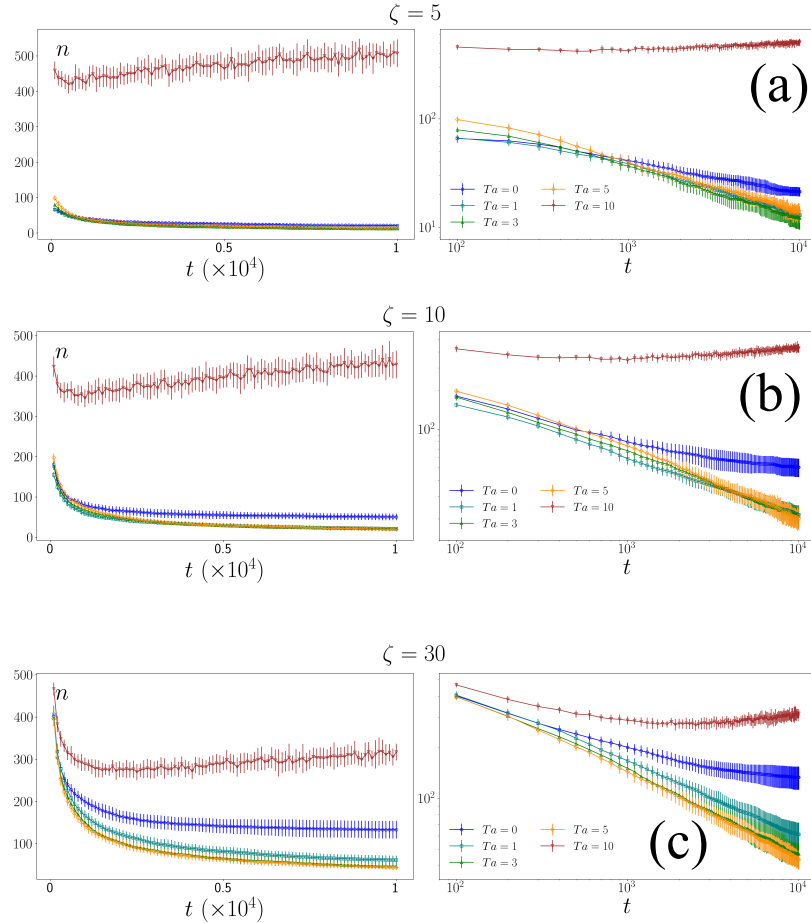


FIG. 1. The figure shows how the number of defects changes with increasing temperature for different values of contractility, System size= 128×128 . (Right) Normal Scale,(Left) log-log scale.

THE EFFECT OF k_2

The parameter k_2 denotes strength of the bending energy cost in the p -field. We vary k_2 from $k_1, 2k_1$ and $3k_1$ where $k_1 = 2.5$. We observe the similar coarsening dynamics of the defects as we increase the strength of the k_2 . We also calculate the intensity distribution for the non-zero values of k_2 as stated above.

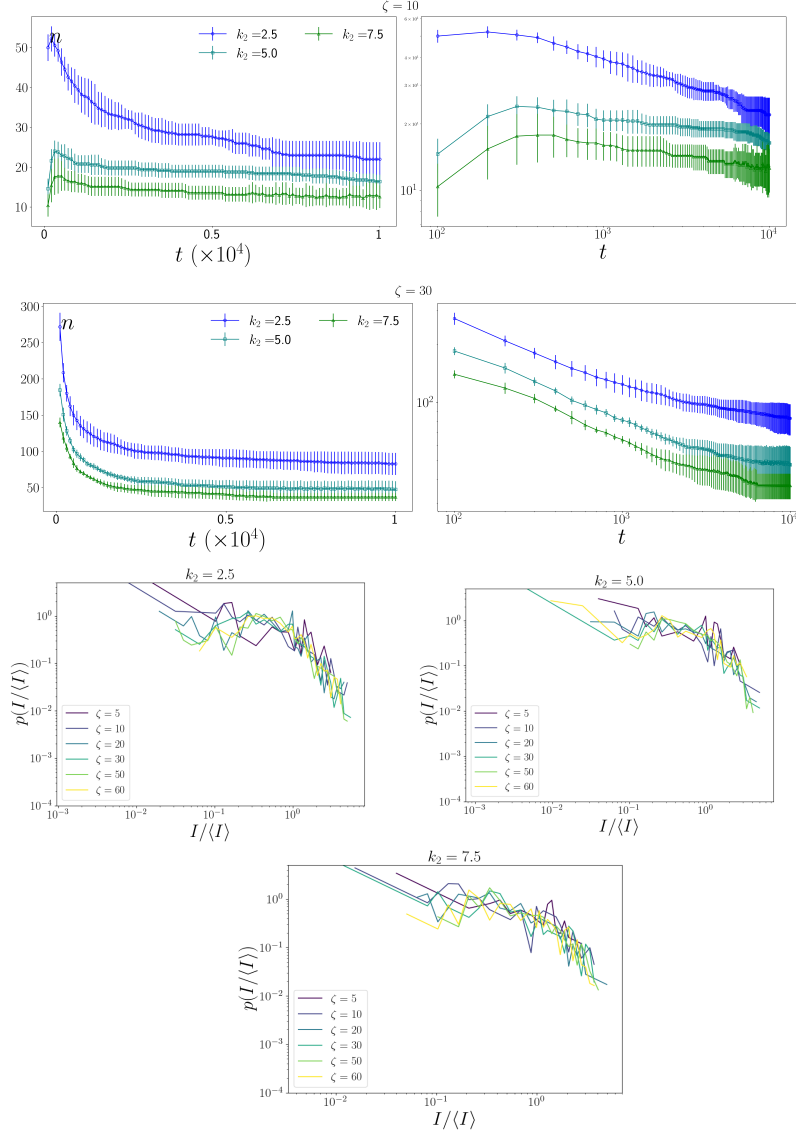


FIG. 2. The figure shows the effect of k_2 and the size distributions for different values of k_2 .

THE EFFECT OF λ

To observe the effect of λ in our system we at first increase the value of λ from $k_1, 2k_1, 3k_1$. Our work is based on the model developed by Gowrishankar et.al. [1, 2] to study the dynamics of actin asters. In these papers, they showed that the aster dynamics is minimally affected by λ and T_a . Specifically, λ changes an inward-pointing aster to a spiral aster[3], and T_a makes the asters more noisy without changing the overall dynamics [1]. However, the nonlinear term involving λ is difficult to integrate numerically. Hence, we have shown the results for a limited range of λ .

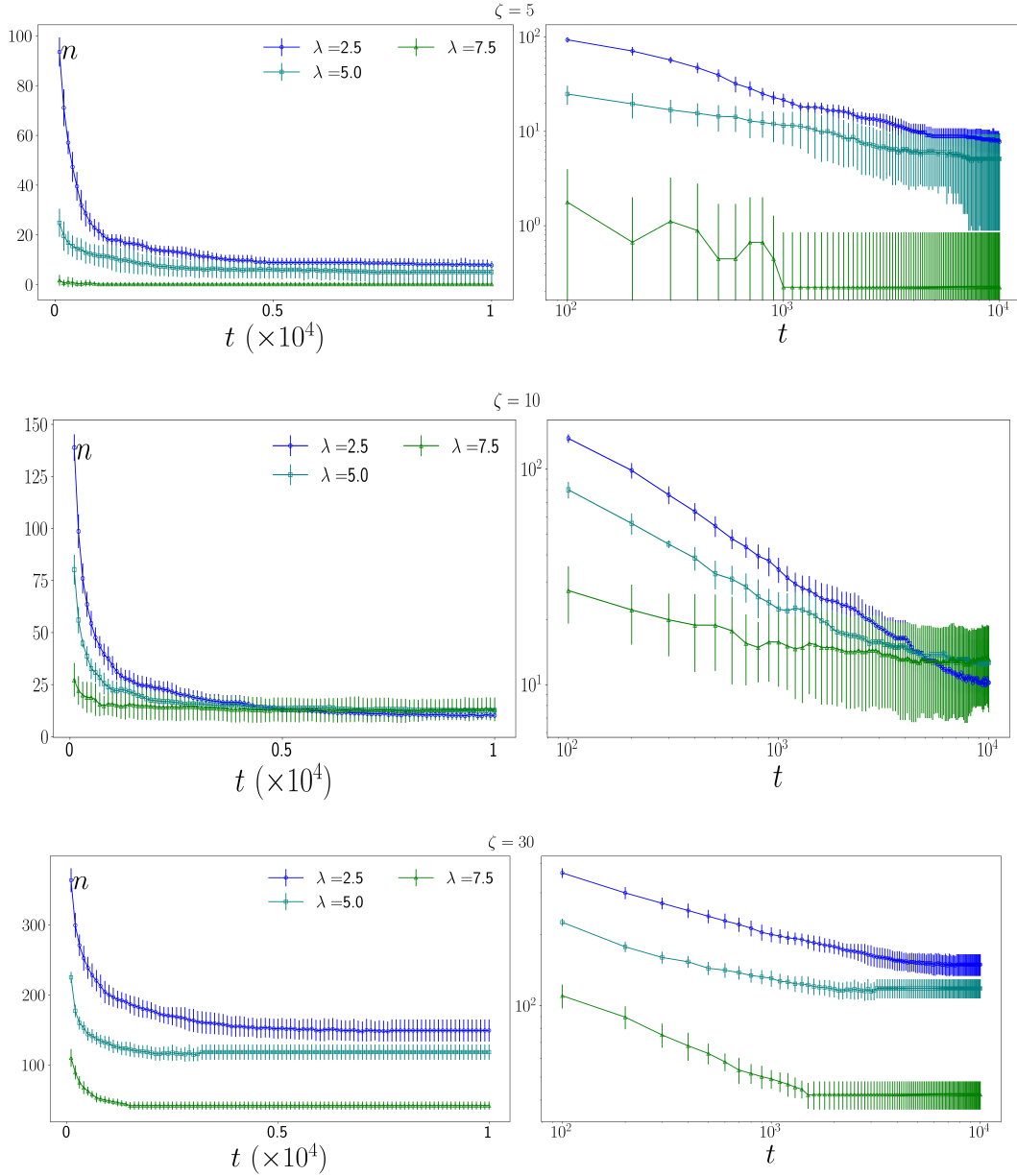


FIG. 3. This figure captures the coarsening dynamics for different values of λ in system size 128×128

CALCULATION OF RADIAL DISTRIBUTION FUNCTION AND POTENTIAL OF MEAN FIELD

We numerically calculate the radial distribution function ($g(r)$) and the potential of mean force defined as $u(r) = -\log(g(r))$ between the defects in the final state. This formula is strictly valid in thermal equilibrium, where $u(r)$ is an estimate of the free energy. In a nonequilibrium system, such as ours, it is unclear what $u(r)$ corresponds to. However, as $T \rightarrow 0$, and the equilibrium system approaches an athermal nonequilibrium system, the free energy can be well approximated by the internal energy. Hence, we also expect $u(r)$ to be an estimate of the interaction energy. As can be seen from the plots below, the location of the minimum of $u(r)$ becomes closer to zero with increasing ζ . This evidence, although not rigorous, supports the claim that activity-dependent screening exists in our system. In the future, we will investigate this question in greater depth, as it currently presents a significant theoretical and numerical challenge.

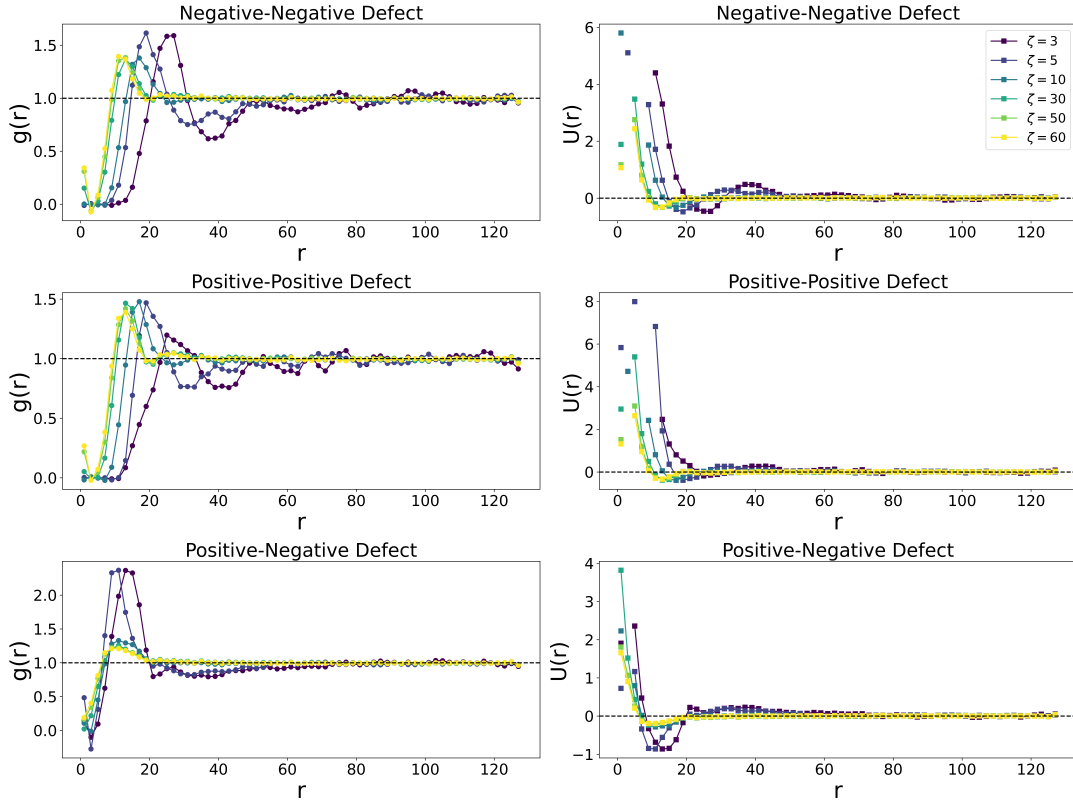


FIG. 4. Calculation of Radial distribution function between defects.

CALCULATION OF THE EVOLUTION OF THE AVERAGE ASTER SIZE DISTRIBUTION OVER TIME

To gain insights about the slow dynamics of our system, we calculate the evolution of average aster size with time. We found out that it reaches a plateau after some timesteps. We also observed that the average sizes decrease with increased values of activity.

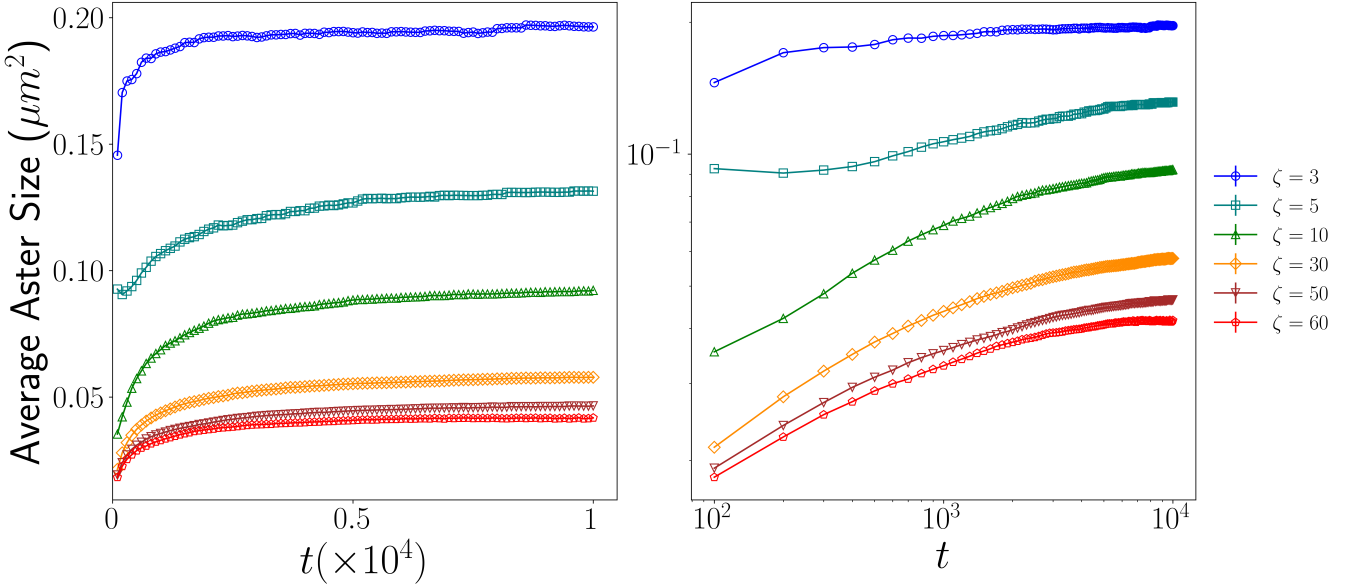


FIG. 5. Number of defects vs Simulation time on log-log scale. (System size = 256×256 , Disorder average=109)

INITIALLY DISORDERED STATE

We also examined the system's behavior under different initial conditions, specifically where the concentration $c = 1 + \delta c$, with $\delta c = 0.01 \times \Gamma$, where Γ is randomly selected from a uniform distribution. Furthermore, the orientation vector $\mathbf{p} = (\cos \theta, \sin \theta)$ is assigned a random angle $\theta \in [0, 2\pi]$, drawn from a uniform distribution. The results were compared with those from our primary simulation, which begins with a homogeneous, ordered initial state. However, simulations starting from a disordered initial state exhibit similar coarsening behavior (Fig. 6). Additionally, we compare the intensity distributions for both scenarios, as shown in Fig. 7.

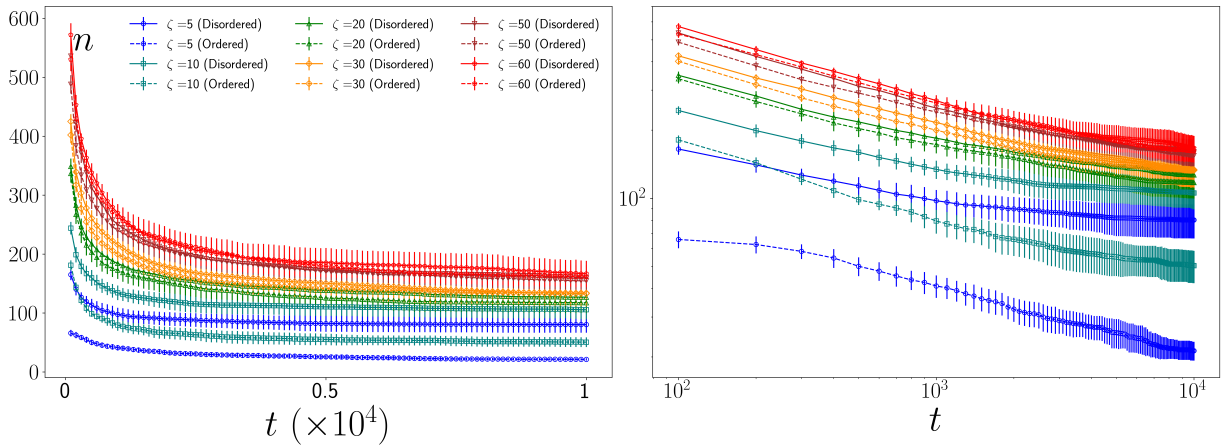


FIG. 6. The figure compares the dynamics of defect coarsening starting from order and disordered state (legend) on a system size = 128×128 and disorder average=20)

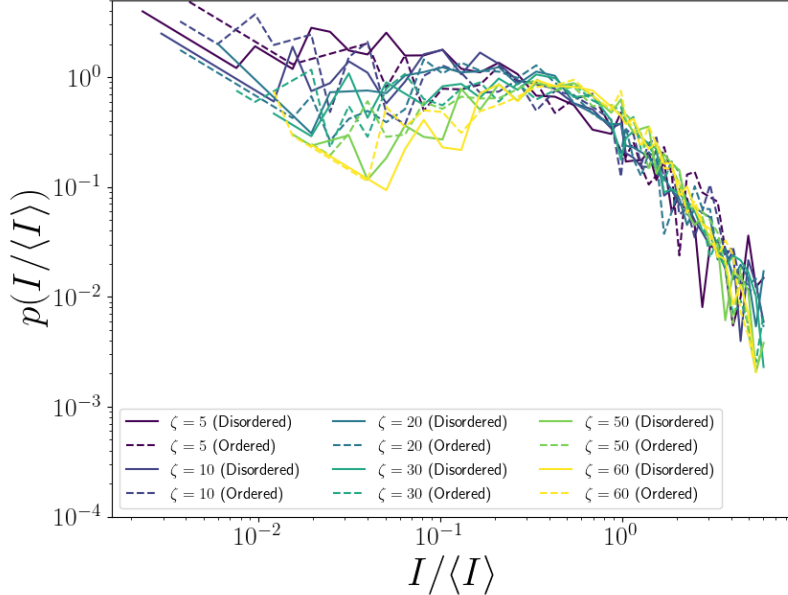


FIG. 7. We calculate the size distribution of the asters starting from an initially disordered state.

DEFECT NUMBER IN LOG-LOG SCALE

In the main text, we plotted the defect number as a function of time using a linear scale (Fig.1(d)). Here, we present the same data using a log-log scale Fig. 8.

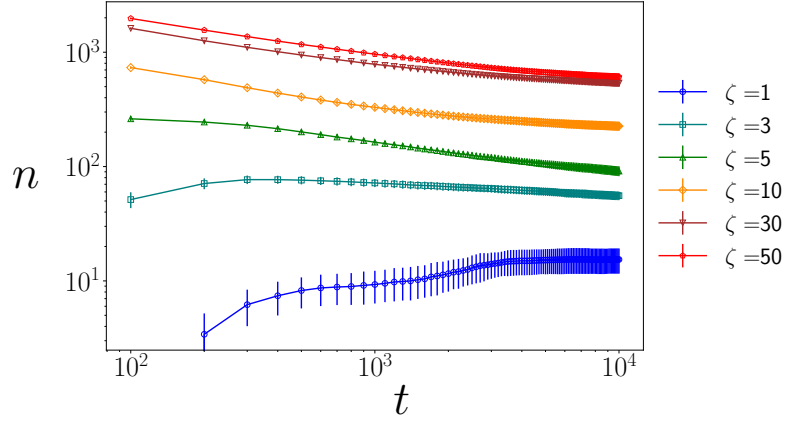


FIG. 8. Defect number as a function of time in log-log scale

SIMULATION RESULTS WITH RK2 TIMESTEP MARCHING

We performed the simulation using the forward in time and central in space (FTCS) method for updating the noise (as it is delta correlated in space and time) term in the Euler-Maruyama scheme. Also, for long-time simulation, there are other methods like the Runge-Kutta second order(RK2) method. We performed the RK2 timestep update for $T_a = 0$ and compared the results (Fig.9 and Fig.10. The results match well in the absence of active temperature (T_a)).

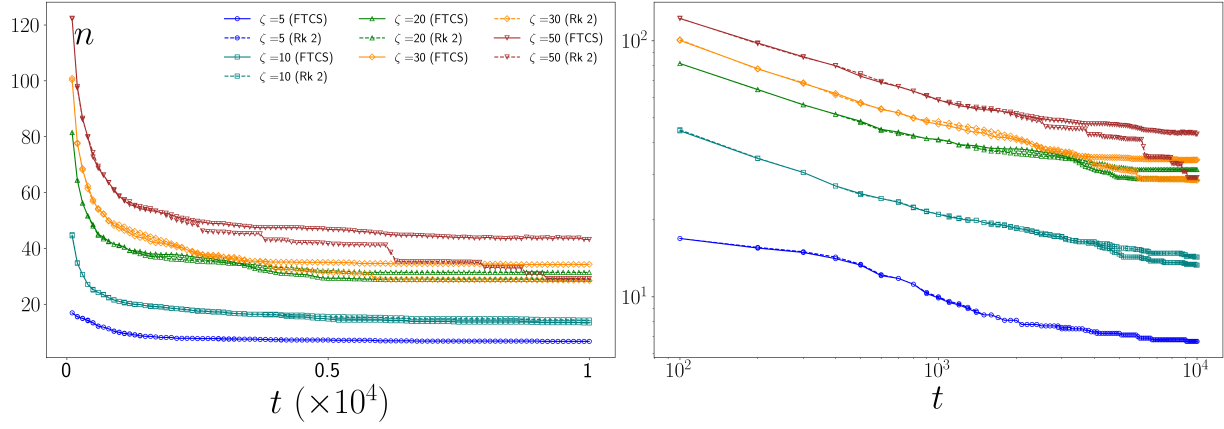


FIG. 9. Comparison of change in a number of defects between the RK2 time marching and the Euler first-order method for time marching. The simulations are done on 64 system size with 20 disorder averages.

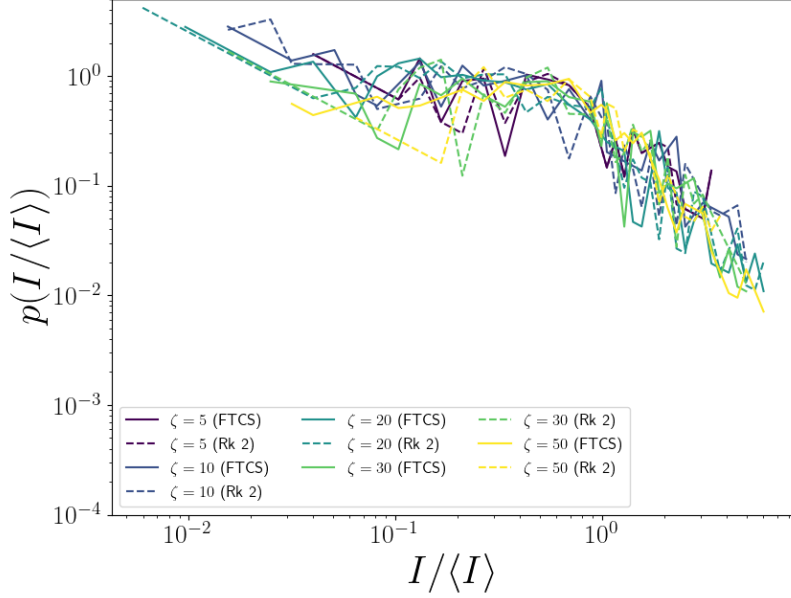


FIG. 10. Comparison of the size distribution of the final state between the RK2 time marching and the Euler first-order method for time marching. The simulations are done on 64 system size with 20 disorder averages.

* msoumyadeep@iisc.ac.in

† pankajpopli@iisc.ac.in

‡ sumantra@iisc.ac.in

- [1] K. Gowrishankar, Active re-modelling of cortical actin regulates spatiotemporal organization of molecules on a living cell surface, *Biophysical Journal* **98**, 304a (2010).
- [2] K. Gowrishankar and M. Rao, Nonequilibrium phase transitions, fluctuations and correlations in an active contractile polar fluid, *Soft matter* **12**, 2040 (2016).
- [3] G. Kripa, *Dynamics of shape and composition of an active composite membrane*, Ph.D. thesis (2012).